ISSN 1070-3632, Russian Journal of General Chemistry, 2015, Vol. 85, No. 5, pp. 1311–1325. © Pleiades Publishing, Ltd., 2015.
Original Russian Text © Yu.D. Korolev, 2013, published in Rossiiskii Khimicheskii Zhurnal, 2013, Vol. 57, Nos. 3–4, pp. 108–120.

Low-Current Discharge Plasma Jets in a Gas Flow. Application of Plasma Jets

Yu. D. Korolev

Institute of High Current Electronics, Siberian Branch, Russian Academy of Sciences, Akademicheskii pr. 2/3, Tomsk, 634055 Russia
e-mail: korolev@lnp.hcei.tsc.ru

Received January 1, 2013

Abstract—The paper describes the results of investigations of low-current discharges in a gas flow at atmospheric pressure. The primary focus is on glow discharges in coaxial plasmatrons and the so-called gliding arc. Such discharges are typically used for obtaining a plasma jet at the exit of the electrode system. The jet contains active chemical species playing an important role in various applications of the discharge. Plasma-assisted combustion and oxidation of hydrocarbon fuels is also considered. Besides, the applications of plasma jet for modification of surfaces and for use in biology and medicine are discussed.

DOI: 10.1134/S1070363215050473

INTRODUCTION

In the electrode system of a gas discharge gap, the flow of gas passes through the discharge zone thus forming a plasma jet inside the system and at the exit of it. A well-known device of this kind is the conventional plasmatron with a coaxial electrode configuretion. An arc plasmatron at a current of 10 A or higher usually generates thermal plasma. Such devices are designed for generating high-temperature plasma jets.

Lately, extensive studies of jets generated by nonequilibrium plasma (glow discharge, corona discharge, dielectric barrier discharge, etc.) have been underway. Usually, total discharge current and current density in such plasma jets are far less than those in the thermal arc, hence, the temperature of the jet at the exit of the electrode system is much lower. Strictly speaking, in these devices it is not a plasma flow that is usually generated; rather, what we get is a certain gas flow of a very low rate of ionization and excitation with chemically active species in the flow. Nevertheless, the term low-temperature "plasma jet" or "plasma plume" is currently widely used in the literature, and we will also use it in this paper.

Major issues of the discharge physics and the possibility of application of non-equilibrium plasma jets are given in review [1]. Currently, various lines of application of discharges continue to develop intensively. The use of discharges in systems for sustaining the combustion and conversion (reforming) of hydrocarbons is an illustrative example [1–9] of it. Of substantial interest is the possibility to use low-temperature plasma jets for modifying surfaces (particularly, surfaces of low-melting dielectrics) [10–15]. Finally, an important field of application is medicine and biology: disinfection, sterilization [16, 17], wound healing [18–22], selective action on cells [18, 19, 23, 24], etc.

The entire realm of research and application of the discharges is too wide to be covered in depth in this paper. Therefore, the data given here belong largely to glow discharges at atmospheric pressure, when there is a constant flow of gas through the discharge zone. Examined here are issues of discharge physics and the major ways of application of plasma jets produced at the exit of the electrode system.

Peculiarities of High-Pressure Glow Discharges

A common property of discharges in a gas flow lies in their being nonsteady-state even in case of a dc power supply. Under the action of a gas flow, the site of plasma column attachment to the surface of the electrodes varies in time, and the length of the column and the discharge-burning voltage change accordingly.

Fluctuations of the discharge-burning voltage within the time scale of about 100 μs is characteristic, in particular, of low-current discharge in a coaxial plasmatron and of the so-called gliding arc. Apart of that, the nonsteady behavior of the discharge occurs within time intervals of about 1 μs and less. This is because we deal here with high-pressure discharges, the fundamental property of which is spontaneous transition from one form of discharge burning to another. For instance, a corona discharge may be accompanied by short high-current pulses and turn into a glow discharge. [25, 26]. A classic low-pressure glow discharge is steady-state. However, at high pressures, a glow-to-spark transition occurs. Usually, the transition is initiated by the development of a specific instability in the near-cathode layer, leading to a microexplosion of the cathode surface and formation of a spark cathode spot [27–32]. Let us examine the issue in more detail.

There is a great variety of discharges that can be described as glow-type. Their common feature is a specific self-organization of the transport of current in the near-cathode region. Near the cathode, there is a zone of voltage drop of l_c length and V_c voltage. V_c is usually above 250 V. The cathode emission current is the result of the photo effect and ion bombardment. This electron current increases on account of the electron multiplication due to ionization within the zone of the cathode voltage drop. The parameters of the cathode region are self-consistently set so that the electron current at the exit of the cathode layer is equal to the current in the plasma column adjoining the layer [27, 33–35].

In case of a self-consistent arrangement of the cathode layer, similarity laws will apply to the near-cathode region of the voltage drop. For a glow discharge, the universal parameter of similarity is the ratio of current density at the cathode surface to squared gas pressure, j/p^2. In the mode of the so-called normal glow discharge, the j/p^2 ratio is constant. Accordingly, in the normal mode of discharge burning, all other parameters of the cathode layer are constant: $V_{cn} = \text{const}_1$, $pl_{cn} = \text{const}_2$, $E_{cn}/p = \text{const}_3$ [34, 35], where E_{cn} is electric field intensity at the cathode surface.

With an increase in the current density, we have an abnormal glow discharge the similarity laws of which show the relation between the ratio of current density to squared gas pressure and other parameters of the layer:

$$V_c = f_1(j/p^2),\ pl_c = f_2(j/p^2),\ E_c/p = f_3(j/p^2). \quad (1)$$

Without going further into the properties of the cathode layer, we must only note that the electric field intensity at the cathode surface rises with increasing j/p^2 ratio. In the same way, even when the j/p^2 parameter remains constant, the field intensity E_c rises with increasing gas pressure. The following parameters are characteristic of the cathode layer of a normal glow discharge in air:

$j_n/p^2 = 230$ μA cm^{-2} Torr^{-2}, $E_{cn}/p \approx 10^3$ V cm^{-1} Torr^{-1} [34].

It is easily seen that at atmospheric pressure and normal current density, the electric field intensity at the cathode gets rather high: E_{cn} = 0.76 mV/cm. The transition to the abnormal discharge mode results in even higher intensity electric fields E_c.

It is the high-intensity electric fields at the cathode layer that facilitate explosive emission instability resulting in a cathode spot [27, 28]. The effect of instability consists in the following [28]: when the electric field intensity at the cathode rises to a certain critical value, microinhomogeneities of the cathode surface begin to produce noticeable field emission; the increase of the current emission from the cathode micropoint leads to a rise of the ion current to that site; as a result, the electric field intensity at the cathode gets higher, thereby further raising the emission current. The process is irreversible and leads to a microexplosion at the cathode surface and formation of a cathode spot.

Early experimental research of the glow-to-spark transition [27, 29–32] were largely motivated by the problem of producing pulsed volume discharges in atmospheric-pressure CO_2 lasers. The underlying principle of ignition of pulsed volume (glow-type) discharges is the idea of multielectron initiation of a discharge [27, 36]. According to this idea, before applying a voltage pulse to the electrodes, a certain concentration of homo-geneously distributed electrons within the electrode gap has to be created. Thereupon, as a result of avalanche electron multiplication, a column of volume discharge will form on a large electrode surface. Using this method, volume discharges of up to hundreds of liters were produced [27, 34].

The duration of volume discharge burning is limited. After a while (within 100 ns to a few μs), the volume discharge turns into a spark one, in other words, contraction of the volume discharge takes place. As noted above, the contraction process is

triggered by the formation of a cathode spot. However, the cathode spot formation does not mean that the transition to the spark channel stage is instantaneous, particularly, when considering the process against a timeline of about 100 ns. The process appears to be multistage [27, 31, 34, 37]. First, a certain part of the volume discharge current is constricted to the cathode spot and a diffuse channel attached to the spot is formed. The conductivity of the diffuse channel is higher than that of the volume discharge plasma column but lower than the conductivity of the spark channel. At the next stage, a constricted (filamentary) high-conductivity spark channel sprouts from the cathode spot along the diffuse channel.

From the data obtained, we can conclude that it is impossible, in principle, to have a steady-state glow discharge at atmospheric pressure. However, in some specific conditions, a glow-discharge current was observed [28, 33, 34, 38, 39]. It concerns, first and foremost, discharges with a small volume of the plasma column, when its diameters of is only ~1 mm or smaller.

Strictly speaking, when applying similarity parameters and laws, it would be more consistent to use not the ratio of electric field intensity to pressure, E/p or j/p^2, but the ratios E/N and j/N^2, where N is the concentration of neutral particles. In the gas discharge physics, the concept of gas pressure is often the equivalent of the concentration of neutral particles [33, 34]. Therewith, a distinction needs to be drawn between gas pressure p in the discharge chamber and certain effective pressure p_{eff} within the region of the gas discharge plasma. Within the plasma region, the gas is heated, and, therefore, due to the small diameter of the plasma column it may lose neutral particles and, as a result, the concentration N of neutral particles in the column becomes lower than that in the discharge chamber. To take this into account, the concept of effective pressure is introduced, which is related to the pressure in the discharge chamber by the equation

$$p_{eff} = p_0(T_0/T), \quad (2)$$

where p_0 = 760 Torr; T_0 = 278 K; and T is the gas temperature within the plasma region.

Therefore, when applying similarity laws, the calculation should include the pressure p_{eff} determined by formula (2).

In a conventional low-pressure glow discharge, gas, virtually, does not heat up, hence $p \approx p_{eff}$. Under atmospheric pressure however, p_{eff} may be several times less than p due to rarefaction of gas within the discharge region. As a result, the field intensity at the cathode surface drops and no explosive emission instability develops at the cathode layer [34]. All this is characteristic of discharges in small-diameter plasma columns.

In view of the aforesaid, it will be useful to look at the results of research on glow discharges in air at atmospheric pressure with the discharge gap d = 1 mm, within the current range i = (0.05 – 0.27) A [39]. It was demonstrated that prior to settling as a steady-state glow discharge, there is a certain time interval of spontaneous transitions from one form of discharge burning to another [39]. Distinguishable are the following stages within that time interval: spark discharge; glow-type discharge without a cathode spot; glow discharge with a cathode spot; discharge with a cathode spot and diffuse channel attached to the cathode spot; formation and spontaneous extinguishing of cathode spots; and short-time current interruptions. On the whole, two important processes take place during the transition time interval: firstly, rarefaction of gas within the discharge region to p_{eff} pressure and, secondly, conditioning of the cathode surface and destruction of micropoints of increased electron emission. Both processes facilitate the burning of a discharge in the steady-state mode.

Typical photographs of steady-state glow discharges are given in Fig. 1 [39]. In the photographs we see the negative glow region of the glow discharge resting, sort of, on the surface of the cathode, a 0.6–0.7-mm discharge column, and the Faraday dark space in between. The diameter of the negative glow region is larger than that of the column, which is usually the case with atmospheric-pressure discharges. With the increase of the discharge current, the diameter of the negative glow region, i.e. the cathode area occupied by the discharge, increases.

Using the current–voltage characteristic of the discharge and measuring the size of the negative glow region, we can estimate the average current density at the cathode. Assuming that the cathode layer is maintained in a normal current–density mode, the j/p_{eff}^2 appears to be a constant value. Basing on this, the effective gas pressure in the negative glow region and gas temperature was determined. As seen from Fig. 2 [39], the effective pressure inside the discharge region is within the range of 120–200 Torr, which is much

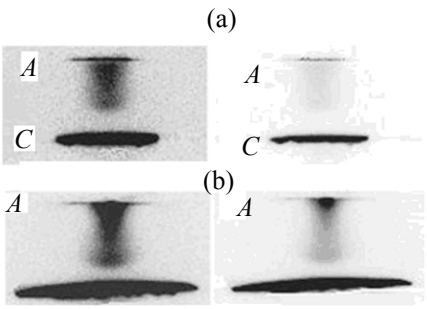

Fig. 1. Photographs of the steady-state atmospheric-pressure glow discharge at the gap distance d = 1 mm: Discharge current (a) i = 0.1 A, burning voltage V_G = 400 V; and (b) i = 0.22 A, V_G = 365 V. (*C*) Gap cathode and (*A*) anode.

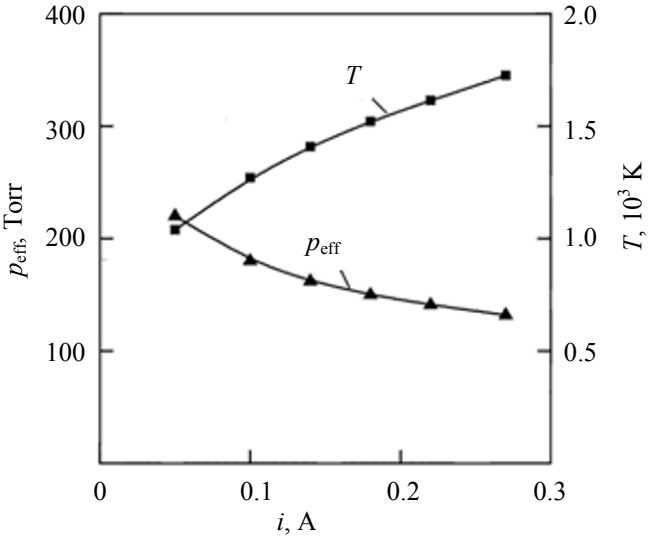

Fig. 2. Dependences of the effective gas pressure and gas temperature on the glow discharge current for the discharge shown in Fig. 1.

less than the initial pressure in the chamber, which allows the glow discharge to be sustained in the steady-state mode without cathode spot formation. However, occasional transitions to the spark discharge mode take place under these conditions as well. Therefore, when the current is a fraction of an ampere and the diameter of the plasma column is less than 1 mm, a steady-state glow discharge can be ignited.

The above-described experiments pertain to conditions, where there is no flow of gas forced through the discharge region. In the presence of a gas flow, the discharge column and the site of its attachment to the electrodes will move together with the flow. Besides, a certain part of charged and excited species may be carried away with the flow, resulting in a low-temperature plasma jet.

Low-Current Discharge in a Coaxial Plasmatron with a Swirling Gas Flow

Coaxial plasmatrons are used for generating discharges and plasma jets in swirling gas flows [3, 4, 8–12, 40–45]. The discharges produced are nonsteady-state due to the flow of gas and glow-to-spark discharge transition. The principle of the plasmatron operation is illustrated in Fig. 3 [40, 41].

The voltage to the cathode of the plasmatron comes from a dc power supply of $V_0 \le 10$ kV via a ballast resistor and a coaxial cable. Typically, the cable capacitance varies within the range of 100–300 pF. When the power supply voltage reaches the value of the static breakdown voltage, the first spark breakdown occurs in the coaxial section of the electrodes. Under the action of a swirling gas flow, the discharge column moves along the coaxial section of the electrodes and finally ends up attached to the end of the cathode and the internal surface of the anode nozzle.

Typically, the air flow rate through the aperture varies within the range of 0.1–1 g/s, whereas the diameter of the aperture is about 4–5 mm. The discharge current may vary with varied power supply voltage and the ballast resistance. As shown in [41], the current flows not only through the discharge column: the air flowing through the plasmatron aperture is weakly ionized, and a certain part of the current is shorted to the anode through this background plasma. In essence, the background plasma is a luminous jet which is seen at the exit of the plasmatron (Fig 3b). When the plasmatron is fed with a mixture of air and propane or methane, then, as a result of combustion, the plasma jet will be longer and its luminosity brighter (Fig. 3c).

The waveforms of current in the plasmatron and of voltage at the electrodes (V_G) demonstrating the instant of discharge ignition in the plasmatron are given in Fig. 4 [40]. The first breakdown forming a channel at the coaxial section of the electrodes happens at time t_1. In the given time scale, the breakdown is accompanied by instantaneous voltage drop at the electrodes. However, if measured within the time interval of about

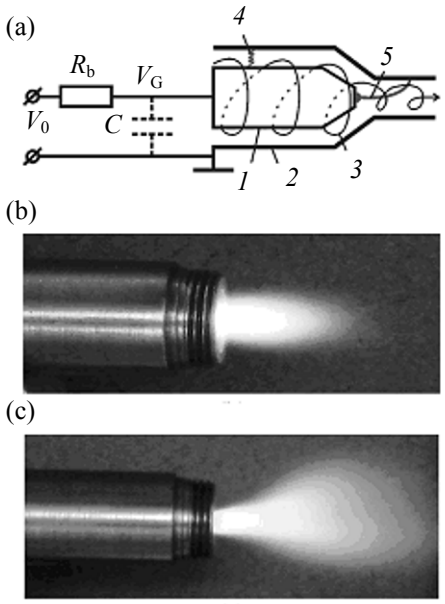

Fig. 3. (a) Schematics of the plasmatron with a swirling gas flow and the plasma jet in (b) air and (c) air–propane mixture: (*1*) cathode; (*2*) anode; (*3*) swirling gas flow; (*4*) position of the spark channel after the first breakdown; (*5*) position of the discharge column at later temporal stages; (R_b) ballast resistance; (V_0) power supply voltage; (V_G) voltage at the plasmatron gap; and (C) capacitance of the connecting cable.

100 ns [40], the breakdown is accompanied by a pulse of oscillating spark current with the oscillation period depending on the capacitance and inductance of the coaxial cable. The cable discharges through the gas discharge gap and the cable energy is released in the spark channel.

After that, the discharge column moves along the coaxial section of the electrodes to the end of the cathode. This stage lasts from instant t_1 to instant t_2. Therewith, discharge burning can take different forms. The cathode spot may be extinguished and the discharge will stay in the glow mode at the burning voltage of about 350 V. Should a cathode spot occur, the discharge burning voltage will drop sharply, and then rise again, when the spot extinguishes. Such sharp rises and drops of the voltage occur within the $t_2 - t_1$ time interval.

By instant of time t_2, the place of attachment of the plasma column to the cathode will be moved to the end of the cathode. The place of the anode attachment continues to move toward the exit from the aperture. The plasma column grows longer and the voltage at the column and gas discharge gap increases, on the

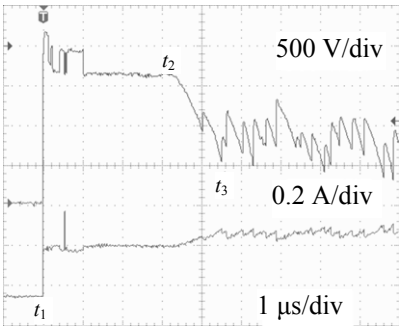

Fig. 4. Voltage and current waveforms for the first breakdown in the plasmatron. The horizontal arrows show zero levels of voltage and current. Gas flow rate G = 0.1 g/s (flow velosity at the plasmatron exit v = 4 m/s); cable capacitance C = 300 pF; ballast resistance R_b = 13.6 kΩ.

whole, accordingly, which can be seen within the t_2 to t_3 time interval. After instant t_3, irregular spikes are seen in the waveforms.

The nature of irregular spikes can be understood if we look at Fig. 5 [40] depicting waveforms for stage $t > t_3$ plotted at a higher time resolution and a photograph of the gas discharge gap luminosity. At this stage, the spatial structure of the discharge consists of a glow discharge column and a background area of a weakly ionized gas within the plasmatron nozzle. The burning of a discharge takes place in the form of glow with random transitions to sparks [40, 41].

We shall consider the process dynamics beginning from a certain instant t_1. By this instant of time, the glow discharge plasma column grew longer, so that the voltage at the gap reaches the value of V_G = 1750 V. The cathode potential drop is about 300 V, meaning that the main fraction of the voltage is applied to the discharge column [39, 40]. At instant t_1 a cathode spot appears, and within the time scale considered the glow discharge undergoes a virtually instantaneous transition into a spark one. The spark discharge channel grows from the electrode end, through the region of a weakly ionized gas and ends up at the internal surface of the anode nozzle.

The energy required for the development of the channel comes from capacitor C charged 1750 V by instant of time t_1. A sharp drop of voltage, virtually, to zero, is accompanied by a discharge current kick. What happened in this specific case was the so-called completed glow-to-spark transition. There turned out to be enough energy stored in the capacitor to form a high-conductivity filamentary (constricted) spark channel (Fig. 5).

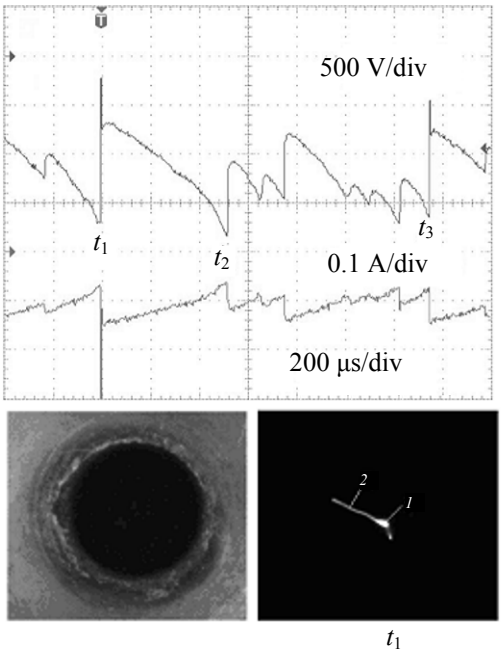

Fig. 5. Voltage and current waveforms for later temporal stages of discharge development and the photograph of the discharge from the plasmatron exit side in the course of the glow-to-spark transition (instant t_1). The photograph on the left shows the plasmatron aperture without discharge. G = 0.1 g/s (v = 20 m/s); C = 300 pF; R_b = 13.6 kΩ, V_0 = 3.0 kV. (*1*) Cathode spot and (*2*) filamentary spark channel.

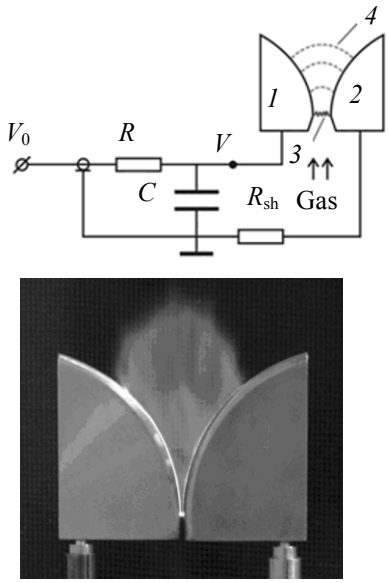

Fig. 6. Schematics of gliding arc ignition and the integral photograph of the discharge in air. Gas flow velocity v = 10 m/s, V_0 = 4 kV, R = 10.3 kΩ, C = 300 pF. (*1*) Cathode; (*2*) anode; (*3*) position of the spark channel after the first breakdown; (*4*) position of the discharge column at later temporal stages, and (R_{sh}) shunt resistance for recording the discharge current.

Following the discharge of the cable capacitance through the gap, the cathode spot extinguishes and the discharge returns to the glow mode. The discharge column grows longer in time and the voltage at the gap increases accordingly up to instant t_2. At instant t_2, the cathode spot appears again and the transition from glow to spark was triggered. However, in this case, it was the so-called noncompleted glow-to-spark transition. There turned out to be not enough energy stored in the capacitor to form high-conductivity filamentary (constricted) spark channel, and, consequently, the process stopped at the stage of the diffuse channel and the cathode spot. The waveform shows a noncompleted voltage drop and a low-amplitude current kick. Completed and noncompleted transitions occur at random. For example, the transition at instant t_3, can be also describe as a completed one.

The results of detailed study of the nonsteady-state behavior of discharges are presented in [39–41]. The overall conclusion to be drawn from the results obtained can be summed up as follows: When current is a fraction of an ampere, a discharge burns in a glow mode with random transitions to sparks. Actually, these are microsparks accompanying energy input of about 1 mJ or less in the discharge channel. As noted in [9, 42], sustaining of combustion of hydrocarbons in a wide range of air–fuel mixtures is provided in this mode. Spark discharges trigger oxidation reaction in a small region of the discharge channel, and the burning process propagates rapidly over space, because the plasmatron aperture area is not a "cold gas" but a weakly ionized medium containing chemically active species.

Gliding arc in a Gas Flow

Another type of discharge whose properties are significantly affected by a gas flow is the so-called gliding arc [46–53]. An electrode system generating gliding arc and its typical power supply circuit are presented in Fig. 6 [48]. The V_0 voltage to the electrodes is supplied from a dc power supply via a ballast resistor and a coaxial cable of C capacitance. In the lower part of the electrode system the electrode gap is the smallest. Therefore, when voltage V_0 reaches a static breakdown value breakdown across the electrode gap occurs and a spark channel *3* appears.

Gas is supplied to the electrode system from the bottom upwards, and the gas flow moves the discharge

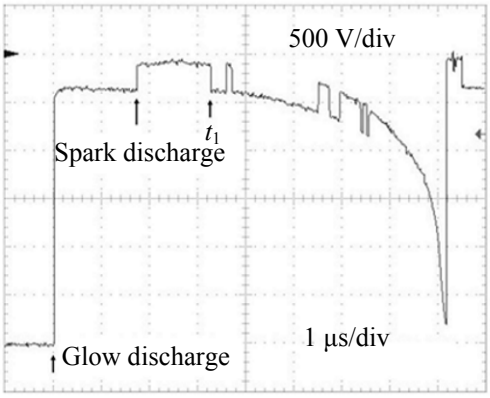

Fig. 7. Voltage waveforms for the gliding arc illustrating discharge development after the first break-down. v = 10 m/s, V_0 = 3 kV, R = 10.3 kΩ, C = 300 pF.

column to position *4* (Fig. 6). The length of the plasma column increases and the plasma voltage rises. At a certain critical voltage, a repeated breakdown at the lower part of electrodes takes place and the plasma column moves upward again. In the integral photograph in Fig. 6 the luminosity of the gas discharge gap appears to be homogeneous. The homogeneity of the image in this case is the result of the spatial movement of the luminous object (small-diameter plasma column) during the exposition.

Apart from dc voltage, bipolar pulsed power sources, for instance, with a pulse frequency of 60 kHz, were used for the described system [49, 52]. Garduno et al. [53] used a source with a 23-kHz pulse frequency. Alternating current supply does not change principally the pattern of primary plasma chemical processes, though it complicates, to a certain degree, visualization and interpretation of the physics involved. Therefore, below we present the results of experiments with dc power supply via a ballast resistor in the discharge circuit.

Pellerin et al. [46] studied discharge in air at a mean current of about 2 A, and proposed a model describing processes within the discharge column. The model is based on the concepts and equations used to describe a positive arc column containing high-temperature neutral species. A good fit to experiment in terms of gas temperature and column conductivity was obtained. It appears that the term "gliding arc" fits the above conditions quite well.

The same approach in the interpretation of the discharge behavior was used by Kuznetsova et al. [47],

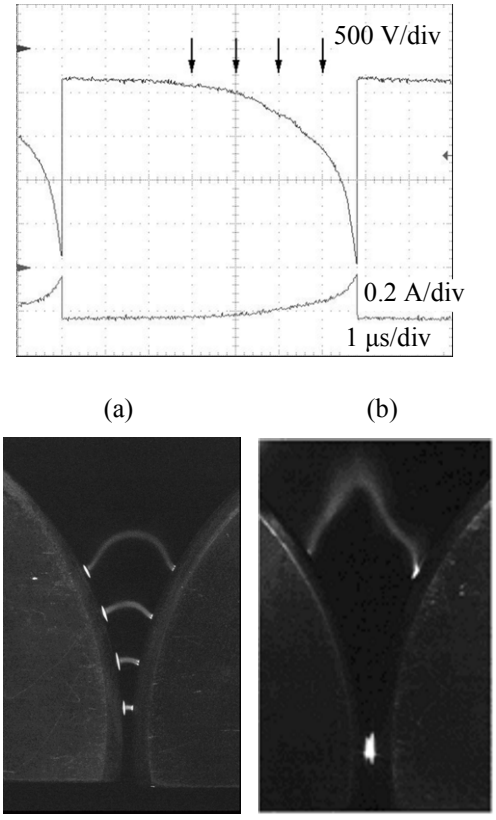

Fig. 8. Voltage and current waveforms and the photographs of the discharge at later temporal stages of gliding arc burning: (a) exposition time Δt = 100 μs, the arrows show the exposition instant; and (b): Δt = 400 μs, the exposition instant t = 6.8 μs corresponds to the repeated breakdown.

though the discharge current there was lower by an order of magnitude than in [46]. As shown above, in a nonsteady-state plasmatron, when the current is a fraction of an ampere, discharge burns in the glow form rather than in the form of an arc with a cathode spot. The same applies to electrodes typical for gliding arc [48].

Figure 7 shows the voltage waveform at the gas discharge gap, which illustrates the development of discharge after the first breakdown [48]. The static breakdown voltage for this electrode system is V_{br} = 3 kV. As a result of the breakdown, a spark channel with a cathode spot appeared in the gap and the cable capacitance discharged less than in 1 μs. Because the current in the circuit is limited by the ballast resistor, the cathode spot cannot be sustained for a long time; it extinguishes and discharge begins to burn in a glow mode. On the timescale of 1 μs/div that swift process of establishing the glow discharge (Fig. 7) is

represented as a sharp drop of voltage from 3 kV to 350 V.

In 1.8 μs a spontaneous drop of the voltage indicating the glow-to-spark transition is seen on the waveform. At instant t_1 the spot extinguishes causing transition to a glow discharge, and so on. On the waveform these spontaneous transitions are reflected as sharp discharge voltage drops and rises. When the discharge column moves together with the gas flow, its length and voltage increase. When the voltage reaches its critical value of about 2.6 kV, another breakdown along the shortest distance at the lower part of electrodes occurs. The voltage of the repeated breakdown is always lower than the static breakdown voltage of V_{br} = 3 kV, because here the cathode at the gap is exposed to radiation from the discharge column. With the repeated breakdown, the voltage at the electrodes drops sharply, recombination decay of the plasma from the column of preceding discharge takes place, and the residual plasma from preceding discharge is blown off the electrode system by the flow of air.

In Fig. 8, together with the current and voltage waveforms of the later stages of the discharge (following the first breakdown), there are photographs of the gas discharge gap. On photograph *a* we can see that the plasma column and its attachments to the cathode and anode move at the velocity of the gas flow. The pattern of glow in the near-cathode region is similar to that shown in Fig. 1. We can see the negative glow region on the surface of the cathode (left column) and another column the diameter of which is smaller than that of the negative glow region.

Estimations carried out in [48] show that under these conditions normal glow discharge is sustained in the gas-discharge gap. The voltage drop at the cathode layer is estimated at about 300 V, and the typical value of the electric field in the plasma column, the length of which is from 0.1 to 3 cm, was in the range of 700–800 V/cm.

Photograph (b) in Fig. 8 was taken with an exposure of 400 μs at the instant of the repeated breakdown in the gap. Seen in the photograph, are the column of preceding discharge and the spark channel in the lower part of the gap during the repeated breakdown. In the model presented by Kuznetsova et al. [47], it was assumed that there was not enough supply voltage to sustain ionization in the lengthening plasma column, hence, the plasma was to decay. It was the sharp increase in the resistance of the gas-discharge gap with the decay of the plasma that was deemed to be the cause of the repeated breakdown. However, the tests have shown that the plasma of the glow-type discharge column does not decay with the elongation of the column, and that the cause of the repeated breakdown is the voltage drop at the electrodes reaching a certain critical value [48].

The same conclusion was made in paper [52] presenting the results of detailed spectroscopic study of the discharge and integral images of glow with space and time resolution.

In general, it would be more appropriate to call the discharge appearing at the current of a fracture of an ampere, with the configuration of electrodes presented in Fig. 6, "gliding glow discharge" rather than "gliding arc;" however, the term "arc" is commonly used in the literature.

Application of Gas Flow Discharges

Plasma-Assisted Combustion and Hydrocarbon Conversion

One of the vigorously developing application fields of plasma is complete or partial oxidation of hydrocarbons using different gas flow discharges and different electrode designs (including coaxial plasmatrons and gliding arc electrode systems) [2–8, 54].

Research in this field is focused on the plasma-assisted pyrolysis of methane into hydrogen and carbon, including carbon in the form of nanotubes [6, 55]. Much attention was given to partial oxidation of methane with air in the presence of water vapor, specifically, steam reforming [4–7, 56]. The partial oxidation is used to obtain hydrogen and syngas (a mixture of CO and H_2):

$$CH_4 + H_2O \rightleftarrows CO + 3H_2 \quad (\Delta H_{298} = 206 \text{ kJ/mol } CH_4), \tag{3}$$

$$CH_4 + 0.5(O_2 + 3.76N_2) \rightleftarrows CO + 2H_2 + 1.88N_2 \quad (\Delta H_{298} = -36 \text{ kJ/mol } CH_4), \tag{4}$$

$$CH_4 + O_2 + 3.76N_2 \rightleftarrows CO_2 + 2H_2 + 3.76N_2 \quad (\Delta H_{298} = -318.9 \text{ kJ/mol } CH_4). \tag{5}$$

Methane pyrolysis, including steam reforming, is an endothermic reaction and, therefore, it requires a lot of energy to occur. Steam reforming is performed using arc plasmatrons which generate a thermal plasma torch [45, 56–58]. For example, Bromberg et al. [56] made use of a coaxial arc plasmatron with water-cooled electrodes. The average power of the

plasmatron was 2–3 kW at typical discharge voltages of 120–160 V. The discharge sustained in an air flow, and methane was supplied to the torch at the plasmatron exit. In the first experiments, the specific energy consumption for hydrogen production was fairly high (W = 270 MJ/kg H_2) [4, 56]. The yields of H_2 and CO were 38 and 65% of the equilibrium yields. Optimization of process conditions allowed the energy consumption to be reduced to 100 MJ/kg H_2 [56].

Further reduction of specific energy consumption (to 45 MJ/kg H_2) was achieved, when the process was performed with an arc plasmatron in a reactor filled with a NiO/Al_2O_3 catalyst. The authors of [56] expect that the regeneration of heat in the reactor may reduce energy consumption to 15–20 MJ/kg H_2. The efficiency of combining systems with an arc discharge and discharges of other types, in particular, a gliding arc electrode configuration, with different catalysts was also studied in [53, 59–61].

The advantage of steam reforming with oxygen is increased hydrogen yield and suppressed formation of nitrogen oxides [4], but, as already noted, the process consumes a lot of energy. This circumstance stimulates research into partial oxidation under steam-free conditions [5–9, 42, 51, 62, 63]. Formally, reactions (4) and (5) are exothermic, but for reasonable reaction rates an external source (discharge) is required. A reasonable option is provided by low-current plasmatrons with glow-type discharges, as well as low-current gliding arc. It should be noted that the nonuniform plasma in this case is formed due to generation of chemically active species rather than by a simple heating of the gas [6, 9, 42, 64, 65]. The low-temperature weakly ionized plasma torch plays the role of a catalyst (the definition "plasma-enhances catalytic oxidation" was even suggested [6, 7, 64, 65]).

When low-current glow discharges, as well as corona and low-current dielectric barrier discharges are used, reagents are fed directly to the plasma region. Discharge considerably extends the range of equivalence ratios which allow the oxidation process to sustain [6, 9, 42, 62, 66]. Thus, in the plasmatron presented in Fig. 3, air oxidation of propane can be performed both in propane-rich fuel mixtures (to obtain syngas) and in air-rich mixtures [42].

This plasmatron was taken as the basis to develop a plasma-assisted combustion system with a high power density per unit area at the exit of the combustion chamber [9, 41–43]. One of the modifications of this

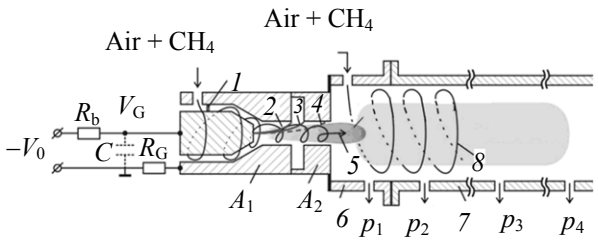

Fig. 9. Schematics of the plasma-assisted combustion system on the basis of a low-current plasmatron: (*1–4*) positions the discharge channel and column in different time moments; (*5*) swirling gas flow through plasmatron; (*6*) intermediate combustion chamber; (*7*) main combustion chamber; and (*8*) swirling gas flow in the combustion chamber.

system (Fig. 9) comprises a low-current plasmatron with a ring-shaped groove at the inner surface of the anode nozzle. Such design suggests that after the glow-to-spark transitions the anode discharge column attaches either to the edge of section A_1 or to the edge of section A_2. Thereafter the current starts flowing mainly to section A_2 [41]. The discharge column occupies positions *2*, *3*, and *4*, which favors a longer discharge column and more efficient interaction of the reaction gas (fuel + air) with plasma. In this system, a two-stage hydro-carbon oxidation concept is realized [9, 42, 43]. A small part of the fuel–air mixtures is fed to the plasma-tron. The power of the generated discharge (60–150 W) [43] is consumed for sustaining at the plasmatron exit of plasma torch/jet with a thermal power of about 1 kW. In its turn, the thermal power of the plasmatron torch is consumed for sustaining combustion of the torch flame in the main combustion chamber. The main part of the fuel–air mixture is fed to the combustion chamber. At typical operation modes, a torch flame was obtained at the chamber exit with a total power of 10 kW and a power density per the unit area of the aperture exit of 1 kW/cm^2. In general, the torch flame suggests diverse applications (in oil sludge combustion systems, sustaining the burning of fuels with a low calorific efficiency or for sustaining various endothermic oxidation processes).

The composition of gas components at different distances from the plasmatron aperture (p_1 – p_4 in Fig. 9) was measured. The role of the plasmatron torch in sustaining the oxidation process is illustrated in Fig. 10 which shows the dependence of the concentration of CO in the exit gas on the air excess coefficient α. In the described experiments, no fuel was fed to the combustion chamber. The equivalence

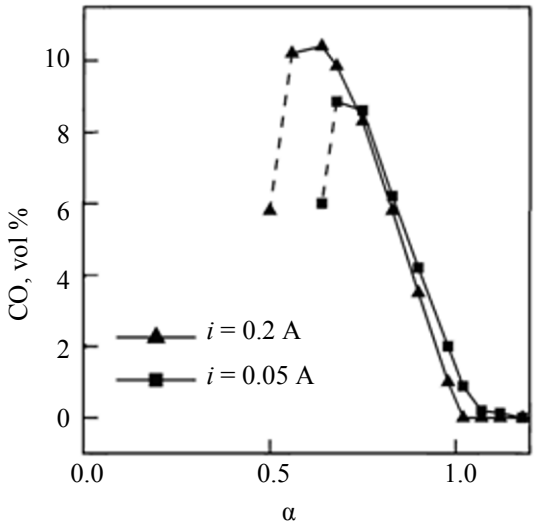

Fig. 10. Dependence of CO content at the plasmatron exit on air excess coefficient α. Air flow rate G = 0.35 g/s; measurements at a distance of 30 cm from the exit nozzle of the plasmatron.

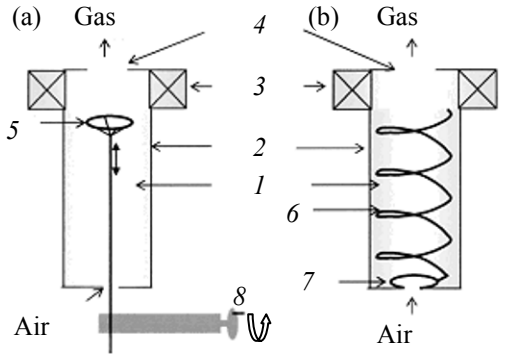

Fig. 11. Schematic representation of gliding arc stabilization in a reverse vortex reactor with (a) ring and (b) spiral electrode configurations: (*1*) reactor volume; (*2*) quartz reactor wall; (*3*) swirler for creation of the reverse vortex flow; (*4*) grounded electrode; (*5*) ring powered electrode; (*6*) spiral powered electrode; (*7*) ring at the tip of the spiral electrode; and (*8*) electrode transporter.

air excess coefficient was varied by introducing methane to a constant air flow. The equivalence ratio α = 1 corresponds to a stoichiometric methane–air mixture (complete methane combustion takes place to form CO_2 and H_2O).

If the composition of the fuel–air mixture is close to stoichiometric, methane burns completely in the immediate vicinity of the exit aperture of the plasmatron. At the distance of 18 cm from the aperture methane burns completely at air excess coefficients of up to 2.8. This value can be considered as an upper burning limit in air for poor fuel–air mixture.

Methane reforming by reactions (4) and (5) is performed in fuel-rich mixtures (α < 1). For the highest yield of syngas the process of partial oxidation should be sustained at low air excess coefficients up to α ≈ 0.25. The example in Fig. 10 shows that plasma almost no longer sustains the oxidation process already at α ≈ 0.5.

Obviously, lower α can be reached by increasing discharge currents, which is possible with an arc plasmatron. However, as mentioned above, the use of arc plasmatrons is associated with fairly high energy consumption [4, 56]. In this connection of interest are the results of Gutsol and co-workers [6, 62], who made use of a gliding arc plasma reactor with the current 0.1–0.2 A for methane reforming to obtain syngas. The two possible schemes of discharge ignition in this reactor are shown in Fig. 11 [62].

The electrode system of the reactor is embedded in a quartz tube (inner diameter 40 mm, height 150 mm). In the system in Fig. 11a, discharge takes place between an energized ring electrode and a grounded electrode (flange). Initially, the electrode gap is set small enough to generate an initial breakdown in the electrode system. After that the electrode gap is increased to make the discharge column nearly as long as the reactor height.

Methane is supplied through a swirler, due to which a swirling gas flow is created. The typical swirl velocities are 10–60 m/s, and the axial gas velocity toward the axis is 2–10 m/s. Air is supplied from the bottom size. Such reactor design ensures efficient interaction of air with the discharge column.

The same gas supply scheme is realized in the system shown in Fig. 11b. The difference is in the design of the energized electrode: it is spiral-shaped. The initial breakdown occurs between the spiral end and the flange. Under the action of the swirling gas flow, the tying site of the discharge column moves along the spiral electrode. As a results, discharge takes place between the flange and ring at the tip of the spiral electrode.

The described reactor was used for methane reforming to obtain syngas [62]. The plasma torch was directed to a heat-insulated chamber. Methane and air are fed through tubes located inside the reactor. The

temperature of the reagents at the reactor inlet is about 700 K.

Under process conditions optimal for this system the methane conversion into syngas was close to 75%. The energy consumption for the production of 1 m^3 of syngas was ~0.1 kW·h. Recalculation of this value into specific consumption for hydrogen production gives W = 4.7 MJ/kg H_2. This appears to be the minimum energy consumption that could be reached at present.

The applications of atmospheric-pressure gliding arc and other low-current discharges in plasma chemistry are not restricted by plasma-assisted hydrocarbon combustion and reforming. Such discharges can also be applied for realization of various reactions, for example, the decomposition of toluene [67, 68]. The gliding arc sustained in gas mixtures in the presence of a water spray was also used for extraction of organic contaminants from solutions [69, 70].

Plasma Surface Modification

One of the application fields of nonsteady-state plasma jets is surface modification [10–15, 71–75] of, in particular, low-melting dielectrics [10, 12–15, 74]. The flux of chemically active species for surface treatment is generally formed in a coaxial plasmatron which can be operated both in glow discharge and corona discharge modes [12, 14, 72, 74, 75]. Dudek et al. [72] described a system formally resembling that in Fig. 3 but having a pin-shaped inner electron. The maximum power supply voltage was 6.5 kV, and the ballast resistance was varied between 100 kΩ to 5 MΩ. The discharge zone responsible for generation of chemically active species in a gas flow is localized near the tip. The species that are considered to contribute most to surface modification are metastable nitrogen molecules. These molecules can be destroyed by oxygen from the surrounding air. Therefore, a laminar gas flow is fed to the plasmatron (maximum rate 17 m/s) to protect the reactive species from air.

Plasmatron with a swirling nitrogen flow (outlet aperture diameter 4 mm, flow rate up to 1 L/s) was used in [12]. The effluent flux is isolated from the surrounding air by means of a glass cylinder at the plasmatron exit. As a result, a 20-cm long plasma jet forms. Such plasma jet treatment improved the hydrophilicity of the deposited polymer film. Research on the elongation of plasma jet is also reported in [73].

The use of coaxial plasmatrons for surface treatment of polymers and cured rubber was described in [10, 11, 74, 75]. Mechanisms responsible for improved wettability and adhesiveness of the treated surface are discussed. Yuji et al. [15] generated plasma jet by means of a microwave (2.45 GHz) discharge.

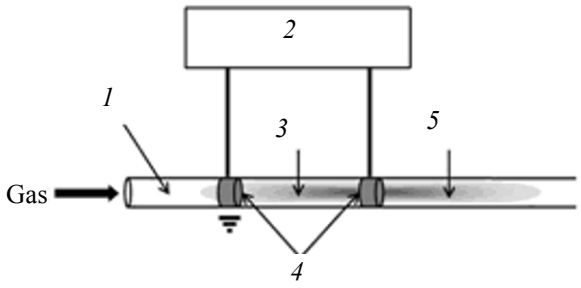

Fig. 12. Schematic representation of plasma jet generation by a dielectric barrier discharge: (*1*) quatz tube; (*2*) power supply; (*3*) discharge; (*4*) electrodes; and (*5*) plasma jet.

Biomedical Applications of Plasma Jets

Discharges in nitrogen–oxygen mixtures are used to obtain nitric oxide NO [43, 76, 77]. At low concentrations it is used in inhalation therapy as a vessel dilator.

The generation of NO in spark discharges at a single spark energy of 0.5–12 J and a pulse frequency of 4.5 Hz is described in [76, 77]. The average energy consumption for the production of one NO molecule was ~600 eV. Using the low-current plasmatron shown in Fig. 3, the energy consumption per one NO molecule could be reduced to 35–50 eV [43].

The plasma jets for medical and biomedical applications contain a great variety of reactive species [nitrogen oxide, ozone, singlet delta oxygen $O_2(^1\Delta)$, etc.], which can react with cells (by suppressing or accelerating cell proliferation), as well as disinfect and heal wounds. The use of different types of discharges and methods of their powering for generation of such plasmas was studied in [18–24, 78, 79].

The schematic of one of reactors for generation of singlet oxygen in He–O_2 mixtures are shown in Fig. 12 [78]. Ring electrodes are located on the outer surface of a quartz tube (outer diameter 6 mm, inner diameter 4 mm). The typical electrode gap is a few cm. The discharge was powered by bipolar pulses with a voltage of up to 10 kV and a frequency of tens of kHz. In essence, here we deal with a dielectric barrier discharge.

In another widely used electrode configuration, the powered electrode is located inside the tube and the grounded electrode is fixed on the outer surface of the

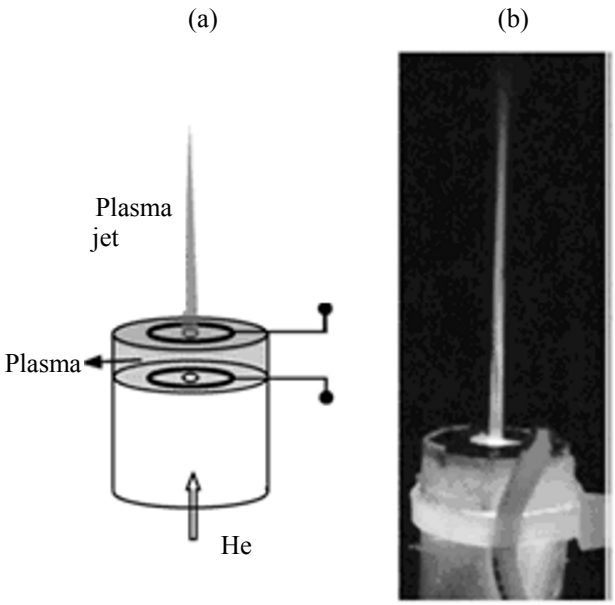

Fig. 13. (a) Schematic representation of plasma microjet generation and (b) photograph of the microjet.

tube. The role of the grounded electrode can also be played by the cylindrical shell with the dielectric tube inserted. Like in the first case, the outer circuit current is provided by the displacement current. Such discharge is sometimes called a single-electrode torch discharge [80]. The design and operation of a miniature source of plasma jet on the basis of a single-electrode torch discharge are presented in [81]. The discharge is powered from a radiofrequency (13.56 MHz) voltage source with a mean power of 1–5 W. The powered inner electrode is inserted into a tube 2 mm in diameter. The plasma jet at the exit of the torch is 0.5 mm in diameter and 2 mm in length. The device is meant for generation of atomic oxygen for cell biology applications.

Alternating current or bipolar pulse single-electrode discharges were also studied in other works. Li et al. [82] described a source in which the inner electrode is pin-shaped. The discharge-feeding voltage frequency is 45 kHz. Bornholdt et al. [83] used a power source with the voltage frequency 1.7 MHz.

Along with the bipolar voltage supplied to the electrode gap, short (normally <1μs) high voltage pulses with a high repetition rate were used for discharge generation. One of such systems is shown in Fig. 13 [84, 85]. A cylindrical dielectric tube (inner diameter 25 mm) is stopped on both ends with dielectric flanges with holes (diameter 3 mm) through which gas is injected with a flow rate of 1–7 L/min. Ring electrodes are located on the outside of the flanges. The voltage of 4.5–7 kV (pulse duration from 200 ns to a few μs, pulse repetition rate up to 10 kHz) is applied to the electrodes

The integral photograph demonstrates a uniform plasma jet at the exit from the system. Spatial and time resolution showed that the jet is not continuous [86, 87]. In fact this is a footprint of the plasma jet emerging from the hole at a rate of 10^6–10^7 cm/s. The authors named this jet the plasma bullet. It was shown that in the case of discharges in mixtures of helium with air the propagation of the plasma jet can be suppressed. Jiang et al. [88] used a similar system to generate a miniature plasma jet.

A specific device for generation of plasma jets similar to that in Fig. 13 was used in [89, 90]. Formally, this device does not contain a grounded electrode, but still it is clear that the discharge current in the external electric circuit was provided due to a parasitic capacitance between the energized electrode and earth.

CONCLUSIONS

At present a certain understanding of the discharge physics has been reached and the application fields of discharges and plasma jets on their basis (plasma-assisted combustion and hydrocarbon reforming, dielectric surface modification, biomedicine) have become discernible. Moreover, some fields of activity, which will receive intensive development in future can be outlined. For example, the term “plasma jet” is fairly common, but the very interaction of gas flow with a discharge plasma column and the physical mechanisms of the formation of plasma jets have scarcely been studied. A deficiency of experimental works focused on the diagnosis of specifically the plasma jet at the exit of the electrode system rather than the discharge column is obvious. It is also obvious that more attention should be paid to the physics of surface modification under the action of plasma jets. Finally, the work on the application of plasma jets in medicine and biomedicine will also be continued.

It appears that the experimental results will be interpreted using computer simulation of discharge, gas dynamic, and plasma chemical processes. At the

same time, the experimental results will allow improvement of the methods of theoretical simulation.

REFERENCES

1. Schutze, A., Leong, J.Y., Babayan, S.E., Park, J., Selwyn, G.S., and Hick, R.F., *IEEE Trans. Plasma Sci*., 1998, vol. 26, no. 6, pp. 1685–1694.
2. Starikovskaia, S.M., *J. Phys. D: Appl. Phys*., 2006, vol. 39, no. 16, pp. R265–R299.
3. Matveev, I.B. and Rosocha, L.A., *IEEE Trans. Plasma Sci*., 2010, vol. 38, no. 12, pp. 3257–3264.
4. Cormier, J.-M. and Rusu, I., *J. Phys. D: Appl. Phys*., 2001, vol. 33, pp. 2798–2803.
5. Petitpas, G., Rollier, J.D., Darmon, A., Gonzalez-Aguilar, J., Metkemeijer, R., and Fulcheri, L., *Int. J. Hydrogen Energ*., 2007, vol. 32, no. 14, pp. 2848–2867.
6. Gutsol, A., Rabinovich, A., and Fridman, A., *J. Phys. D: Appl. Phys*., 2011, vol. 44, no. 27, article no. 274001.
7. Babariotskii, A.I., Deminskii, M.A., Demkin, A.I., Zhivotov, V.K., Potapkin, B.V., Poteknin, S.V., Rusanov, V.D., Ryzantsev, E.I., and Etievan, C., *High Energ. Chem*., 1999, vol. 33, no. 1, pp. 45–51.
8. Tao, X.M., Bai, M.G., Li, X., Long, H., Shang, S., Yin, Y.X., and Dai, X.Y., *Prog. Energ. Combust. Sci*., 2011, vol. 37, pp. 113–124.
9. Korolev, Y.D., Frants, O.B., Landl, N.V., Geyman, V.G., Shemyakin, I.A., Enenko, A.A., and Matveev, I.B., *IEEE Trans. Plasma Sci*., 2009, vol. 37, no. 12, pp. 2314–2320.
10. Noeske, M., Degenhardt, J., Strudthoff, S., and Lommatzsch, U., *Int. J. Adhes. Adhes*., 2004, vol. 24, no. 2, pp. 171–177.
11. Romero-Sanchez, M.D. and Martin-Martinez, J.M., *Int. J. Adhes. Adhes*., 2006, vol. 26, no. 5, pp. 345–354.
12. Takemura, Y., Yamaguchi, N., and Hara, T., *Jpn. J. Appl. Phys*., 2008, vol. 47, no. 7, pp. 5644–5647.
13. Kropke, S., Akishev, Y.S., and Hollander, A., *Surf. Coat. Technol*., 2001, vol. 142, pp. 512–516.
14. Leduc, V, Coulombe, S., and Leask, R.L., *IEEE Trans. Plasma Sci*., 2009, vol. 37, no. 6, pp. 927–933.
15. Yuji, T., Urayama, T., Fujii, S., Mungkung, N., and Akatsuka, H., *Surf. Coat. Technol*., 2008, vol. 202, nos. 22–23, pp. 5289–5292.
16. Montie, T.C., Kelly-Wintenberg, K., and Roth, J.R., *IEEE Trans. Plasma Sci*., 2000, vol. 28, no. 1, pp. 41–50.
17. Cooper, M., Fridman, G., Staack, D., Gutsol, A.F., Vasilets, V.N., Anandan, S., Cho, Y.I., Fridman, A., and Tsapin, A., I *IEEE Trans. Plasma Sci*., 2009, vol. 37, no. 6, pp. 866–871.
18. Laroussi, M., *IEEE Trans. Plasma Sci*., 2009, vol. 37, no. 6, pp. 714–725.
19. Kolb, J.F., Mohamed, A.-A.H., Price, R.O., Swanson, R.J., Bowman, A., Chiavarini, R.L., Stacey, M., and Schoenbach, K.H., *Appl. Phys. Lett*., 2008, vol. 92, no. 24, article no. 241501.
20. Kuhn, S., Bibinov, N., Gesche R., and Awakowicz, P., *Plasma Sources Sci. Technol*., 2010, vol. 19, no. 1, article no. 015013.
21. Kuo, S.P., Chen, C.Y., Lin, C.S., and Chiang, S.H., *IEEE Trans. Plasma Sci*., 2010, vol. 38, no. 8, pp. 1908–1914.
22. Duarte, S., Kuo, S.P., Murata, R.M., Chen, C.Y., Saxena, D., Huang, K.J., and Popovic, S., *Phys. Plasmas*, 2011, vol. 18, article no. 073503.
23. Yan, X., Zou, F., Zhao, S., Lu, X.P., He, G., Xiong, Z., Xiong, Q., Zhao, Q., Deng, P., Huang, J., and Yang, G., *IEEE Trans. Plasma Sci*., 2010, vol. 38, no. 9, pp. 2451–2457.
24. Wende, K., Landsberg, K., Lindequist, U., Weltmann, K.D., and Woedtke, T., *IEEE Trans. Plasma Sci*., 2010, vol. 38, no. 9, pp. 2479–2485.
25. Akishev, Y.S., Grushin, M.E., Kochetov, I.V., Napartovich, A.P., Pan'kin, M.V., and Trushkin, N.I., *Plasma Phys. Rep*., 2000, vol. 26, no. 2, pp. 157–163.
26. Janda, M., Martisovits, V., and Machala, Z., *Plasma Sources Sci. Technol*., 2011, vol. 20, no. 3, article no. 035015.
27. Mesyats, G.A. and Korolev, Y.D., *Usp. Fiz. Nauk*, 1986, vol. 148, no. 1, pp. 101–122.
28. Kozyrev, A.V., Korolev, Y.D., and Mesyats, G.A., *Zh. Tekh. Fiz*., 1987, vol. 57, no. 1, pp. 58–64.
29. Kozyrev, A.V., Korolev, Y.D., Mesyats, G.A., Novoselov, Y.N., and Shemyakin, I.A., *Zh. Tekh. Fiz*., 1981, vol. 51, no. 9, pp. 1817–1822.
30. Korolev, Y.D., Mesyats, G.A., and Khuzeev, A.P., *Dokl. Akad. Nauk SSSR*, 1980, vol. 253, no. 3, pp. 606–609.
31. Korolev, Y.D., Kuzmin, V.A., and Mesyats, G.A., *Zh. Tekh. Fiz*., 1980, vol. 50, no. 4, pp. 699–704.
32. Genkin, S.A., Korolev, Y.D., and Khuzeev, A.P., *Zh. Tekh. Fiz*., 1982, vol. 52, no. 5, pp. 875–879.
33. Meek, J.M. and Craggs, J.D., *Electrical Breakdown of Gases*, Oxford: Clarendon, 1953.
34. Korolev, Y.D. and Mesyats, G.A., *Physics of Pulsed Breakdown in Gases*, Yekaterinburg: Ural Branch, Russian Academy of Sciences, 1998.
35. Kozhevnikov, V.Y., Kozyrev, A.V., and Korolev, Y.D., *Plasma Phys. Rep*., 2006, vol. 32, no. 11, pp. 949–959.
36. Genkin, S.A., Karlov, N.V., Klimenko, K.A., Korolev, Y.D., Kuzmin, V.A., Mesyats, G.A., Novoselov, Y.N., and Prokhorov, A.M., *Pis'ma Zh. Tekh. Fiz*., 1984, vol. 10, no. 11, pp. 641–645.
37. Kozyrev, A.V. and Korolev, Y.D., *Zh. Tekh. Fiz*., 1981, vol. 51, no. 10, pp. 2210–2213.
38. Becker, K., Schoenbach, K., and Eden, J., *J. Phys. D: Appl. Phys*., 2006, vol. 39, no. 3, pp. R55–R70.
39. Korolev, Y.D., Frants, O.B., Geyman, V.G., Kasyanov, V.S.,

and Landl, N.V., *IEEE Trans. Plasma Sci*., 2012, vol. 40, no. 11, pp. 2951–2960.

40. Korolev, Y.D., Frants, O.B., Landl, N.V., Geyman, V.G., and Matveev, I.B., *IEEE Trans. Plasma Sci*., 2007, vol. 35, no. 6, pp. 1651–1657.
41. Korolev, Y.D., Frants, O.B., Landl, N.V., Geyman, V.G., and Matveev, I.B., *IEEE Trans. Plasma Sci*., 2009, vol. 37, no. 4, pp. 586–592.
42. Korolev, Y.D., Frants, O.B., Landl, N.V., Kasyanov, V.S., Galanov, S.I., Sidorova, O.I., Kim, Y., Rosocha, L.A., and Matveev, I.B., *IEEE Trans. Plasma Sci*., 2012, vol. 40, no. 2, pp. 535–542.
43. Korolev, Y.D., Frants, O.B., Landl, N.V., and Suslov, A.I., *IEEE Trans. Plasma Sci*., 2012, vol. 40, no. 11, pp. 2837–2842.
44. Rao, X., Hammack, S., Carter, C., Matveev, I.B., and Lee, T., *IEEE Trans. Plasma Sci*., 2010, vol. 38, no. 12, pp. 3265–3271.
45. Askarova, A.S., Karpenko, E.I., Lavrishcheva, Y.I., Messerle, V.E., and Ustimenko, A.B., *IEEE Trans. Plasma Sci*., 2007, vol. 35, no. 6, pp. 1607–1616.
46. Pellerin, S., Richard, F., Chapelle, J., Cormier, J.-M., and Musiol, K., *J. Phys. D: Appl. Phys*., 2000, vol. 33, pp. 2407–2419.
47. Kuznetsova, I.V., Kalashnikov, N.Y., Gutsol, A.F., Fridman, A.F., and Kennedy, L.A., *J. Appl. Phys*., 2002, vol. 92, no. 8, pp. 4231–4237.
48. Korolev, Y.D., Frants, O.B., Geyman, V.G., Landl, N.V., and Kasyanov, V.S., *IEEE Trans. Plasma Sci*., 2011, vol. 39, no. 12, pp. 3319–3325.
49. Zhang, C., Shao, T., Xu, J., Ma, H., Duan, L., Ren, C., and Yan, P., *IEEE Trans. Plasma Sci*., 2012, vol. 40, no. 11, pp. 2843–2849.
50. Xu, G.F. and Ding, X.W., *IEEE Trans. Plasma Sci*., 2012, vol. 40, no. 12, pp. 3458–3464.
51. Sagas, J.S., Neto, A.H., Pereira, A.C., Maciel, H.C., and Lacava, P.T., *IEEE Trans. Plasma Sci*., 2011, vol. 39, no. 2, pp. 775–780.
52. Sun, Z.W., Zhu, J.J., Li, Z.S., Adlen, M., Leipold, E., Salewski, M., and Kusano, Y., *Optic Express*, 2013, vol. 21, no. 5, pp. 6028–6044.
53. Garduno, M., Pacheco, M., Pacheco, J., Valdivia, R., Santana, A., Lefort, B., Estrada, N., and Rivera-Rodrıguez, C., J. *Renew. Sustain. Energ*., 2012, vol. 4, article no. 021202.
54. Kosarev, I.N., Aleksandrov, N.L., Kindysheva, S.V., Starikovskaia, S.M., and Starikovskii, A.Y., *J. Phys. D: Appl. Phys*., 2008, vol. 41, no. 3, article no. 032002.
55. Korolev, Y.D., Frants, O.B., Landl, N.V., Geyman, V.G., Zerlitsyn, A.G., Shiyan, V.P., and Medvedev, Y.V., *IEEE Trans. Plasma Sci*., 2009, vol. 37, no. 12, pp. 2298–2302.
56. Bromberg, L., Cohn, D.R., Rabinovich, A., O'Brien, C., and Hochgreb, S., *Energ. Fuels*, 1998, vol. 12, no. 1, pp. 11–18.
57. Artemov, A.V., Bul'ba, V.A. Voshchinin, S.A., Krutyakov, Y.A., Kudrinskii, A.A., Ostryi, I.I., and Pereslavtsev, A.V., *Russ. J. Gen. Chem*., 2012, vol. 82, no. 4, pp. 791–800.
58. Artemov, A.V., Bul'ba, V.A. Voshchinin, S.A., Krutyakov, Y.A., Kudrinskii, A.A., Ostryi, I.I., and Pereslavtsev, A.V., *Russ. J. Gen. Chem*., 2012, vol. 82, no. 4, pp. 801–807.
59. Rafiq, M.H. and Hustad, J.E., *Renew. Energ*., 2011, vol. 36, no. 11, pp. 2878–2887.
60. Lee, H. and Sekiguchi, H., *J. Phys. D: Appl. Phys*., 2011, vol. 44, no. 27, article no. 274008.
61. Pornmai, K., Jindanin, A., Sekiguchi, H., and Chavadej, S., *Plasma Chem. Plasma Process*, 2012, vol. 32, no. 4, pp. 723–742.
62. Karla, C.S., Gutsol, A.F., and Fridman, A.F., *IEEE Trans. Plasma Sci*., 2005, vol. 33, no. 1, pp. 32–41.
63. Levko, D.S., Tsymbalyuk, A.N., and Shchedrin, A.I., *Plasma Phys. Rep*., 2012, vol. 38, no. 11, pp. 913–923.
64. Babaritskii, A.I., Baranov, I.E., Bibikov, M.B., Demkin, S.A., Zhivotov, V.K., Konovalov, G.M., Lysov, G.V., Moskovskii, A.S., Rusanov, V.D., Smirnov, R.V., and Cheban'kov, F.N., *High Energ. Chem*., 2004, vol. 38, no. 6, pp. 407–410.
65. Rusanov, V.D., Babaritskii, A.I., Baranov, I.E., Bibikov, M.B., Deminskii, M.A., Demkin, S.A., Zhivotov, V.K., Konovalov, G.M., Lysov, G.V., Moskovskii, A.S., Potapkin, B.V., Smirnov, R.V., and Cheban'kov, F.N., *Dokl. Chem*., 2004, vol. 395, pp. 82–85.
66. Hwang, N., Lee, J., Lee, D.H., and Song, Y.H., *Plasma Chem. Plasma Process*., 2012, vol. 32, no. 2, pp. 187–200.
67. Du, C.M., Yan, J.H., and Cheron, B., *Plasma Sources Sci. Technol*., 2007, vol. 16, pp. 791–797.
68. Trushkin, A.N., Grushin, M.E., Kochetov, I.V., Trushkin, N.I, and Akishev, Y.S., *Plasma Phys. Rep*., 2013, vol. 39, no. 2, pp. 167–182.
69. Burlica, R. and Locke, B.R., *IEEE Trans. Ind. Appl*., 2008, vol. 44, no. 2, pp. 482–489.
70. Tu, X., Yu, L., Yan, J.H., Cen, K.F., and Cheron, B.G., *Phys. Plasmas*, 2009, vol. 16, article no. 113506.
71. Korolev, Y.D., Mesyats, G.A., and Yarosh, A.M., *High Energ. Chem*., 1987, vol. 21, no. 5, pp. 389–392.
72. Dudek, D, Bibinov, N., Engemann, J., and Awakowicz, P., *J. Phys. D: Appl. Phys*., 2007, vol. 40, no. 23, pp. 7367–7371.
73. Hsu, C.C. and Yang, J.J., *IEEE Trans. Plasma Sci*., 2009, vol. 38, no. 3, pp. 496–499.
74. Lommatzsch, U., Pasedag, D., Baalmann, A., Elling-

horst, G., and Wagner, H.E., *Plasma Process. Polym*., 2007, vol. 4, no. 1, pp. S1041–S1045.

75. Martin-Martinez, J.M. and Romero-Sanchez, M.D., *Eur. Phys. J. Appl. Phys*., 2006, vol. 34, pp. 125–138.
76. Namihira, T., Tsukamoto, S., Wang, D.Y., Katsuki, S., Hackam, R., Okamoto, K., and Akiyama, H., *IEEE Trans. Plasma Sci*., 2000, vol. 28, no. 1, pp. 109–114.
77. Sakai, S., Matsuda, M., Wang, D., Namihira, T., Akiyama, H., Okamoto, K., and Toda, K., *Acta Phys. Pol. A*, 2009, vol. 115, no. 6, pp. 1104–1106.
78. Sousa, J.S., Niemi, K., Cox, L.J., Algwari, Q. T., Gans, T., and O'Connell, D., *J. Appl. Phys*., 2011, vol. 109, no. 12, article no. 123302.
79. Ionin, A.A., Kochetov, I.V., Napartovich, A.P., and Yuryshev, N.N., *J. Appl. Phys*., 2007, vol. 40, no. 2, pp. R25–R61.
80. Vlasov, V.A., Tikhomirov, I.A., and Lutsenko, Y.Y., *Physics and Electro-Physics of High-Frequency Torch Discharge and Plasmatrons on Its Base*, Tomsk–Northampton: STT, 2007.
81. Leveille, V. and Coulombe, S., *Plasma Sources Sci. Technol*., 2005, vol. 14, pp. 467–476.
82. Li, S.Z., Huang, W.T., and Wang, D., *Phys. Plasmas*, 2009, vol. 16, article no. 093501.
83. Bornholdt, S., Wolter, M., and Kersten, H., *Eur. Phys. J. D*, 2010, vol. 60, no. 3, pp. 653–660.
84. Laroussi, M. and Lu, X., *Appl. Phys. Lett*., 2005, vol. 87, article no. 113902.
85. Karakas, E., Koklu, M., and Laroussi, M., *J. Phys. D: Appl. Phys*., 2010, vol. 43, article no. 155202.
86. Karakas, E. and Laroussi, M., *J. Appl. Phys*., 2010, vol. 108, article no. 063305.
87. Jarrige, J., Laroussi, M., and Karakas, E., *Plasma Sources Sci. Technol*., 2010, vol. 19, no. 6, article no. 065005.
88. Jiang, C., Chen, M.T., and Gundersen, M.A., *J. Phys. D: Appl. Phys*., 2009, vol. 42, article no. 232002.
89. Xiong, Q., Lu, X., Ostrikov, K., Xiong, Z., Xian, Y., Zhou, F., Zou, C., Hu, J., Gong, W., and Jiang, Z., *Phys. Plasmas*, 2009, vol. 16, no. 4, article no. 043505.
90. Lu, X., Xiong, Q., Xiong, Z., Hu, J., Zhou, F., Gong, W., Xian, Y., Zou, C., Tang, Z., Jiang, Z., and Pan, Y., *J. Appl. Phys*., 2009, vol. 105, article no. 043304.